International Journal of
Computing and
Engineering
(IJCE)

Design and Analysis of Multi-layer Resistive Ink Film Based Met material Ultra-thin Broadband Absorber

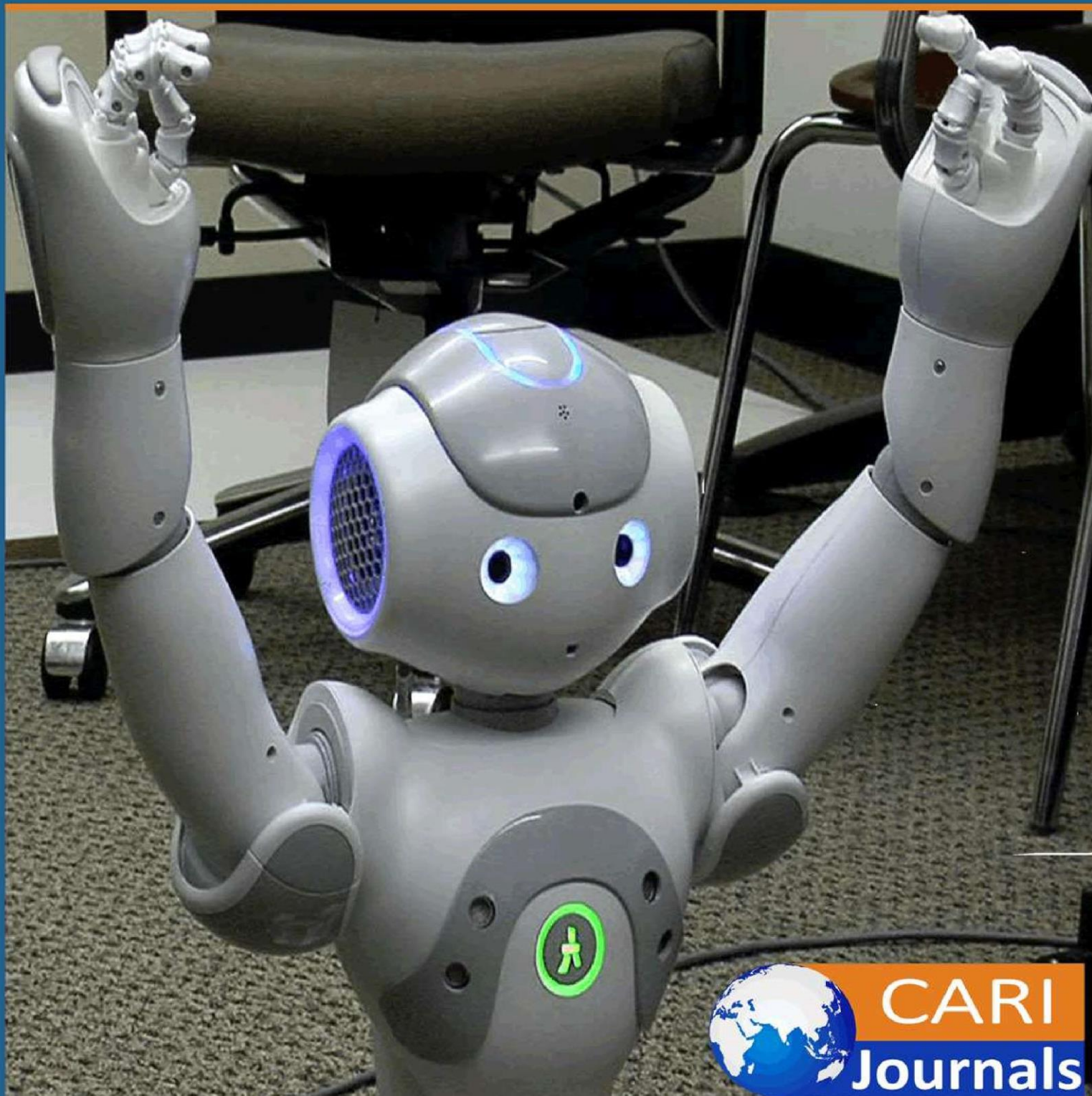

CARI Journals

International Journal of Computing and Engineering
ISSN 2958-7425 (online)
Vol. 5, Issue No. 4, pp. 27 - 43, 2024
www.carijournals.org

Design and Analysis of Multi-layer Resistive Ink Film Based Metamaterial Ultra-thin Broadband Absorber

[1*] Osman M. Alsemaid, [2] A. Awad Babiker, [3] E. Sulieman Saad

[1*, 2, 3] Karary University

https://orcid.org/0009-0005-6135-2442

Accepted: 5th Mar, 2024 Received in Revised Form: 5th Apr, 2024 Published: 5th May, 2024

Abstract

Purpose*:* In order to achieve an excellent electromagnetic absorption response for radar applications, this work proposes a design of an ultra-thin, super broadband, high efficiency meta-material that is insensitive to incidence angle.

Methodology*:* a metamaterial based on multilayer resistive ink unit cell is selected, designed and optimized for minimum electromagnetic absorption and widest bandwidth. The equivalent circuit is derived and analyzed and compered using matlab to results from electromagnetic simulator CST.

Findings*:* Calculating approval requires impedance matching in the structure, which makes it challenging to absorb at high frequencies. In this instance, the proposed structure achieves more than 0.98 absorptivity between 4 and 400 GHz, resulting in a broad absorption bandwidth. When exposed to oblique incidences, the proposed structure behaves in the same way for both transverse electric (TE) and transverse magnetic (TM) modes up to 45°. The total thickness of the planned absorber is 2.105 mm, or 0.028 λ0 at the lowest working frequency. Additionally, find and compare previous radar band reports with the proposed absorber. It is reported to offer more practical feasibility and to be a viable choice for S, C, X, Ku, K, Ka, V, and W bands in addition to millimeter-band radar applications.

Unique contribution to theory, practice and policy*:* Increasing the band width compared to previous studies while increasing the absorption efficiency and reducing the thickness of the metamaterial.

Keywords: *Metamaterial, Resistive Ink , Broadband.*

Introduction

Meta-materials are manufactured materials with exceptional electromagnetic properties that are not present in natural materials. These characteristics result from the material's sub-wavelength structure, which enables exact control over how it reacts to incoming electromagnetic waves. With even more customization options for their electromagnetic behavior, multi-layered meta-material structures are well suited for use in radar cross section reduction, cloaking devices, antennas, and sensors, among other things.

In 1967, V. G. Veselago investigated theoretically the interaction of a plane wave on a material with negative permittivity and permeability (Veselago, 1968) . He believed that such a homogeneous material could be fabricated with a semiconductor. There was no technology to fabricate such a material then, and his work was ignored. It was not until twenty-nine years later that J. B. Pendry revisited V. G. Veselago's theory and published a paper about an artificial metallic construction that exhibited negative relative permittivity εr (Pendry, Holden, Stewart, & Youngs, 1996) . In 2001, Smith (Shelby, Smith, Nemat-Nasser, & Schultz, 2001) conducted a demonstration that a structure consisting of split-ring resonators (SRR) and wires can represent V. G. Veselago's theory. From then on, interest in MTMs grew.

In a material environment that has been precisely constructed, a reduction in scattering cross-sections causes things to be less detectable and, if scattering is nonexistent, may finally produce "invisible" objects. Due to the ongoing need to become invisible to visible light (Cai, Chettiar, Kildishev, & Shalaev, 2007; Gabrielli, Cardenas, Poitras, & Lipson, 2009; Valentine, Li, Zentgraf, Bartal, & Zhang, 2009) and radar waves (Schurig et al., 2006) the idea of "cloaking" was first suggested in (Farhat, Guenneau, Movchan, & Enoch, 2008; Pendry, Schurig, & Smith, 2006). Either conformal optical mapping of complex electromagnetic potentials (Farhat et al., 2008) or transformation optics principles (Pendry et al., 2006) are used in generic cloaking techniques. The second approach necessitates a position-dependent variation in the refractive index, whereas the former often demands highly anisotropic (and occasionally solitary) electric and magnetic susceptibilities of a medium of a cloak.

The reduction of inherent material losses and the minimization of permeability and anisotropy requirements are two major problems in the creation of effective cloaking devices. Through the application of quasi-conformal mapping and the imposition of specific geometrical constraints, the so-called "carpet cloak" has been developed and put into practice to alleviate these issues (Landy & Padilla, 2009; J. Li & Pendry, 2008).

Applications for electromagnetic (EM) wave absorbers abound, including stealth technologies (Kim, Han, & Hahn, 2017), regarding anechoic chambers EM compatibility (Yang et al., 2017) , (Shi et al., 2018) ,shielding against EM interference Reduction of radar cross section (RCS) by (Sista, Dwarapudi, Kumar, Sinha, & Moon, 2021) Onward, (Zhu et al., 2022). The first known radar absorber is the Salisbury screen, which consists of a resistive plate positioned at a quarter wavelength in front of a conductive plate. The Salisbury screen offers a

limited absorption bandwidth despite its straightforward construction. The Jaumann absorber with extra resistive sheets was introduced to broaden the Salisbury screen's absorption bandwidth. Nonetheless (Yao, Xiao, Li, & Wang, 2020), (Su et al., 2022) reported an increase in the Jaumann absorber's overall thickness.

Radar absorber applications are increasingly dependent on broadband, tiny thickness, and robust absorption due to the electromagnetic equipment's and the sensing system's wide working frequency range (Huang et al., 2021), (M. Li, Muneer, Yi, & Zhu, 2018), (Soheilifar & Zarrabi, 2019) and (Lin et al., 2021).

To increase the absorption bandwidth in the past, Ferrites lumped circuits and multiple resonators were employed. The radar absorbers are designed using the circuit analog technique, which further increases the absorption bandwidth. These lossy components, which can be lumped resistors (S.-J. Li et al., 2018), resistive ink (Wang, Ding, He, Mao, & Ruan, 2022), or periodically ordered conductive patterns, make up these circuit analog absorbers. Absorption is achieved across a wide frequency range by adjusting the properties of the resistive conductive top surface.

For S, C, X, Ku, K, Ka, V, W, and millimeter band applications, this paper suggests a multi-layer, super broadband, ultra-thin, and insensitive to wide incidence angle radar absorber using resistive ink. Furthermore, we have conducted a functional comparison between our work and recently published absorbers that are relevant in terms of operating band, absorption efficiency, relative bandwidth, bandwidth ratio, and thickness.

Theory and Design

The suggested absorber's side and three-dimensional views are shown in Figs. 1(a) through 1(d). The multi-layer resistive film technique is employed in the absorber design to increase the absorption bandwidth. Thus, three layers of resistive ink over polymethacrylimide (PMI) foam make up the unit cell of the proposed absorber shown in Fig. 1(a). Its substrates are considered to be PMI foam material, with a loss tangent (tan δ) value of 0.002 and a relative dielectric constant (ε_r) of 1.06. Assuming copper for its ground plane, its electrical conductivity (σ) is 5.96×10^7 S/m. The resistance on the surface of the three layers, resistive ink is selected with R = 300Ω/square.

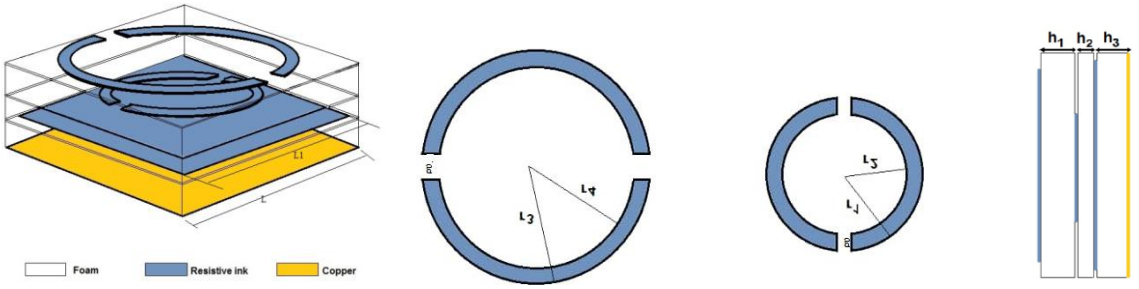

(a) (b) (c)

Figure 1 Unit cell structure: (a) 3D view, (b) Top layer including, design dimensions, (c) Middle layer including design dimensions, (d) Side view.

Table 1 Dimensions of Designed Absorber.

parameters	L_1(mm)	L_2 (mm)	r_1(mm)	r_2(mm)	r_3(mm)	r_4(mm)	g(mm)	h_1(mm)	h_2(mm)	h_3(mm)	t(mm)
values	6	5.5	2	1.5	2.6	2.1	1	0.5	0.5	2	0.035

The suggested absorber is positioned in the x-y plane, where waves travel in the z-direction, during the simulation that uses the frequency domain solver in CST.

The magnetic field (H), electric field (E), and propagation direction (k) are shown here by the x, y, and z directions, respectively.

The metal sheet's surface resistance and the air's wave impedance need to match for optimal absorption outcomes. It is possible to express the meta-material's absorption with impedance matching as follows:

$$A(\omega) = 1 - R(\omega) - T(\omega) = 1 - |S_{11}(\omega)|^2 - |S_{21}(\omega)|^2 \quad (1)$$

where the transmittance is $T(\omega)$, the absorbance is $R(\omega)$, and the absorbance is $A(\omega)$. $S_{11}(\omega)$ and $S_{21}(\omega)$, two frequency-dependent S-parameters, are used to derive the reflectance and transmittance, respectively. Since $|S_{21}(\omega)|^2$ is about zero, as illustrated in Fig. 2, the transmittance is approximately zero. Because of this, absorption is written as:

$$A(\omega) = 1 - R(\omega) \quad (2)$$

$$R(\omega) = \left| \frac{Z_{in}(\omega) - Z_0}{Z_{in}(\omega) + Z_0} \right| \quad (3)$$

$$R_{TE}(\omega) = \frac{Z(\omega)\cos\theta_i - Z_0\cos\theta_t}{Z(\omega)\cos\theta_i + Z_0\cos\theta_t} \quad (4)$$

$$R_{TM}(\omega) = \frac{Z(\omega)\cos\theta_t - Z_0\cos\theta_i}{Z(\omega)\cos\theta_t + Z_0\cos\theta_i} \quad (5)$$

where Z_0 represents the frequency-dependent free space characteristic impedance and $Z_{in}(\omega)$ represents the frequency-dependent characteristic input impedance.

The real and imaginary components of the normalized input impedance should be around 1 and 0, respectively, to achieve impedance matching in the operational band. The definition of the normalized input impedance (Z) is as follows:

$$Z = \sqrt{\frac{(1+S_{11})^2 - S_{21}^2}{(1-S_{11})^2 - S_{21}^2}} = \frac{1+S_{11}}{1-S_{11}} \tag{6}$$

The following equations must be used to study the physical mechanism in order to determine the electromagnetic parameters (permittivity and permeability) using S_{11} parameters:

$$\varepsilon_{eff} = 1 + \frac{2j(S_{11}-1)}{k_0 d(S_{11}+1)} \tag{7}$$

$$\mu_{eff} = 1 + \frac{2j(S_{11}+1)}{k_0 d(S_{11}-1)} \tag{8}$$

where d is the absorber material's thickness and k_0 is the wave number. Understanding whether absorption is electrical or magnetic resonance (or both) depends on these electromagnetic properties.

Simulation Results And Analysis

Matlab 2019 and CST Microwave Studio 2021are used to simulate and to evaluate the suggested absorber's performance and efficiency. It automatically chooses the number of networks per unit wavelength. In the frequency domain, the study of tetrahedral mesh type was used.

Though it concurs on raising the bandwidth and absorption, the study is in line with earlier research. Table 2 displays the comparisons made between the study and earlier research.

It can be seen that the suggested design is a radar absorber in Fig. 2 given that the parameter S_{21} is nearly zero throughout the whole frequency range. The Fig. 3 shows the suggested meta-material's absorption value. A substrate thickness of 0.028λ0 allows for high absorption covering the S, C, X, Ku, K, Ka, V, W, and millimeter bands. Six different absorption peaks with 0.9988 percent or more absorption efficiency are reached at 15.8 GHz, 63.3 GHz, 190.4 GHz, 240.2 GHz, 339.8 GHz, and 396.4GHz. Based on peak frequency values, the corresponding maximum absorptivity percentage is 0.9996, 0.9993, 0.9999, 0.9988, 0.9999, and 0.9997, respectively. Fig.4a illustrates the equivalent circuit of the designed unit cell and Fig.4b illustrates its performance in terms of frequency versus absorbitivity. Fig.5 illustrates the different θ_{in}^{TE} , ϕ_{in}^{TE} , θ_{in}^{TM} and ϕ_{in}^{TM} . The absorption efficiency of the planned meta-material at operational frequencies is unaffected by the values in ϕ_{in}^{TE} and ϕ_{in}^{TM} . Put differently for θ_{in}^{TE} and θ_{in}^{TM} , the absorption performance of the designed metamaterial is larger than 0.95 up to 400 GHz.

The real and imaginary components of ε_{eff} and μ_{eff}, respectively, are depicted in Fig.6. We obtain positive real effective permittivity values in the 4-400 GHz range based on the results of these parameters, allowing the suggested absorber to react to an applied external field. As a result, magnetic resonance serves as the main driving force behind the proposed absorber.

In order to have a deeper understanding of the proposed absorber's performance for $\theta_{in}^{TE}, \theta_{in}^{TM}$, more investigation is conducted. Fig.5 displays the absorption efficiencies under the TE and TM modes based on variations in incidence angles. Fig.5 depict absorbency lines, whereas Fig.4 provide examples of contour plots. The suggested absorber can function over incidence angles up to 45 thanks to the proposed meta-material's strong absorbency, which is above 95%. As a result, it can be concluded that the suggested absorber is insensitive above the absorption reference level.

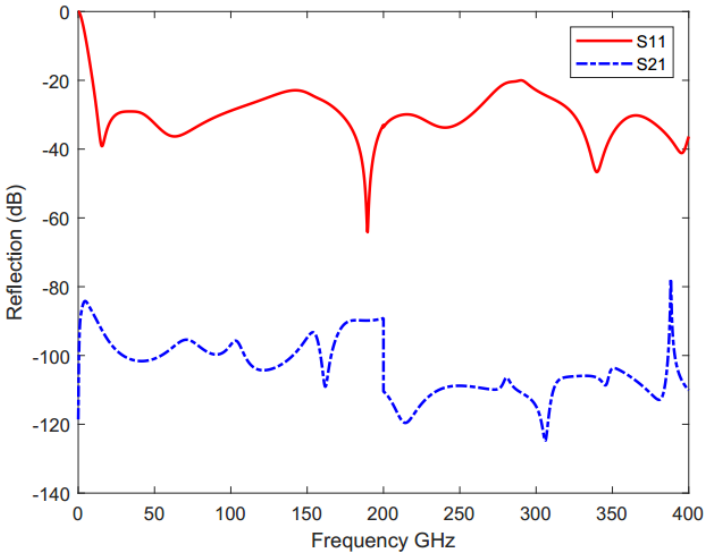

Figure 2 Reflection and transmission coefficients of the proposed absorber.

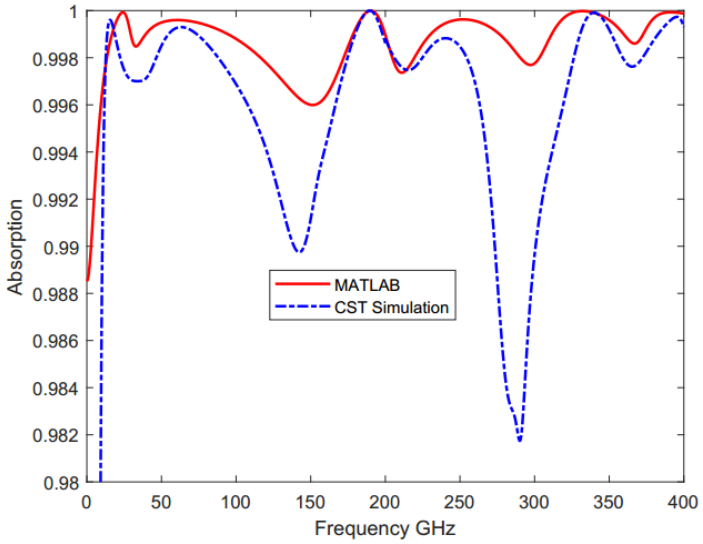

Figure 3 Absorption efficiency of the proposed absorber.

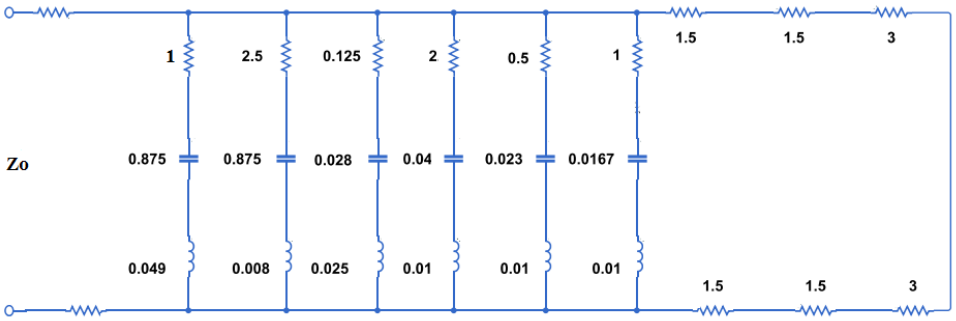

(a)

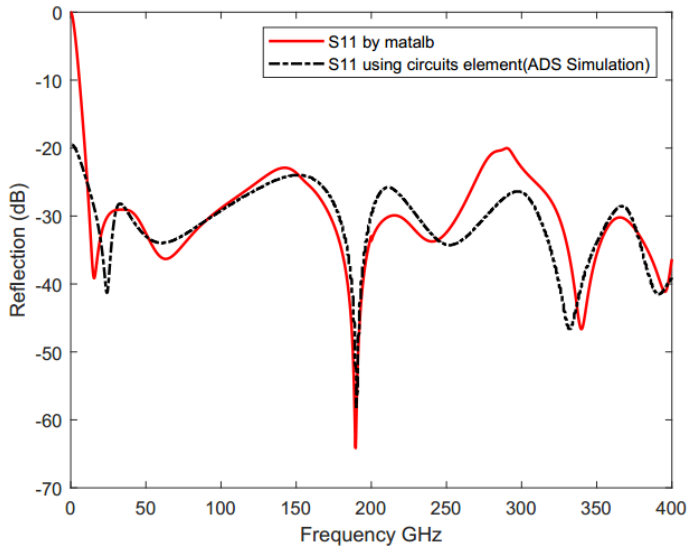

(b)

Figure 4 (a) Equivalent circuit of design (b) Reflection coefficient from equivalent circuit compared with Matlab

Fig.7 and Fig.8 show the values of permittivity and permeability in TE and TM mode at different values of incidence angle, It is apparent that depending on the frequency, the values of permittivity and permeability change from positive to negative and vice versa, indicating that the design is of the CRLH meta-material type.

The relative absorption bandwidth (RBW) is 196.04% based on the predicted absorption exceeding 99 percent. Equation 9, which defines the absorption performance of the suggested absorber, is calculated, with f_L and f_U representing the lower and upper frequencies, respectively. In this case, the lower (f_L) and upper (f_U) frequencies are 4 GHz and 400 GHz, respectively.

$$RBW = 2.\frac{f_U - f_L}{f_U + f_L} \tag{9}$$

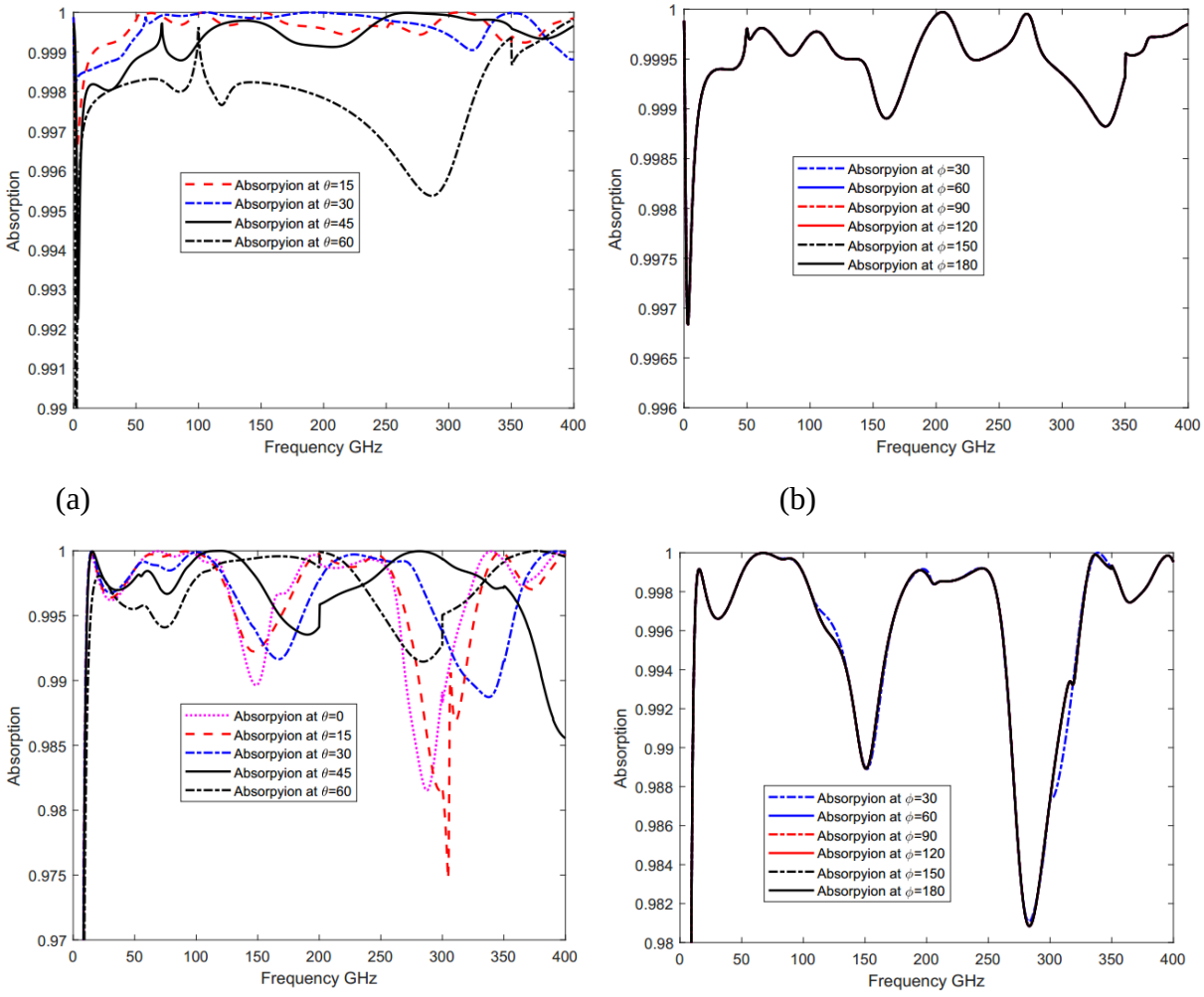

Figure 5 Absorption efficiencies of the proposed absorber for

(a) $\theta_{in}^{TE} = 15,30,45 and 60$ (b) $\phi_{in}^{TE} = 30,60,90,120,150 and 120$

(c) $\theta_{in}^{TM} = 0,15,30,45 and 60$ (d) $\phi_{in}^{TM} = 30,60,90,120,150 and 120$

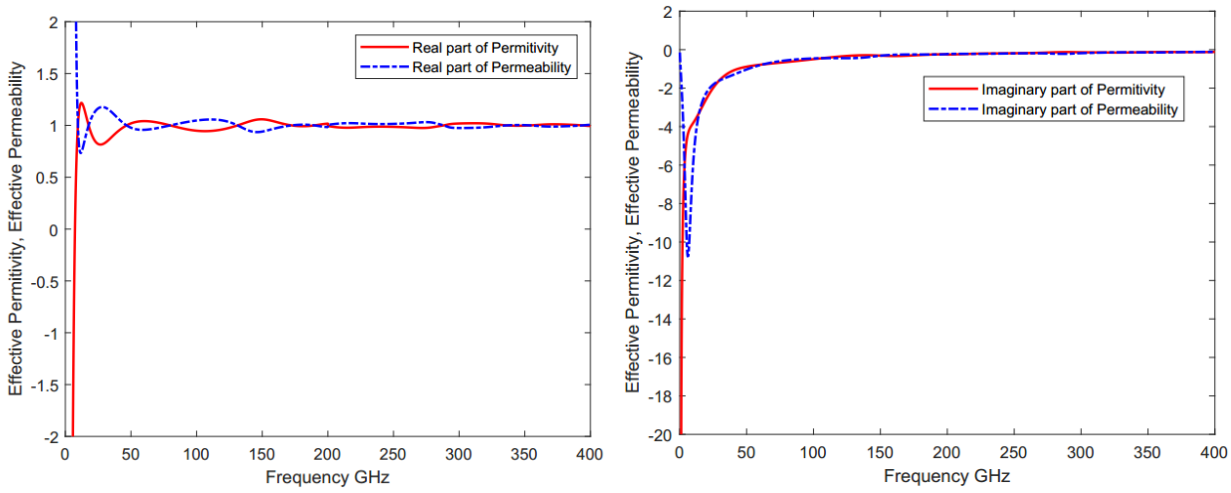

(a) (b)

Figure 6 Extracted electromagnetic constitutive parameters at normal incidence (a)real part of permittivity and permeability (b) imaginary part of permittivity and permeability

The confirmation of impedance matching based on f_L and f_U in Fig. 9, Fig. 10, and Fig. 11 is provided by the approximate values of 1 and 0, respectively, for the real part of impedance and imaginary part of impedance components of the normalized input effective impedance.

The effective medium hypothesis states that meta-materials can be thought of as with the aid of electromagnetic constitutive characteristics. The majority of research in the easily readable literature has focused on Re(ϵ) and Re(μ), whereas the lowest values of imag(ϵ) and imag(μ) may be reached to reduce losses and provide an ideal absorber. Even positive permeability media, including positive permeability values, can be produced with significant absorbency. The mechanism of absorption can be understood in terms of excited magnetic resonances controlling absorbency almost without reflections. An understanding of the physics underlying the super broadband absorption mechanism is provided by the values of extracted electromagnetic constitutive parameters (Fig. 9, Fig. 10, and Fig. 11). We determine positive actual effective permeability values based on these characteristics, allowing the suggested absorber to react to an externally applied field. Furthermore, it produces a magnetic dipole in opposition to an applied external field. Consequently, it may be concluded that the primary motivation for the suggested absorber is magnetic resonance.

International Journal of Computing and Engineering
ISSN 2958-7425 (online)
Vol. 5, Issue No. 4, pp. 27 - 43, 2024
www.carijournals.org

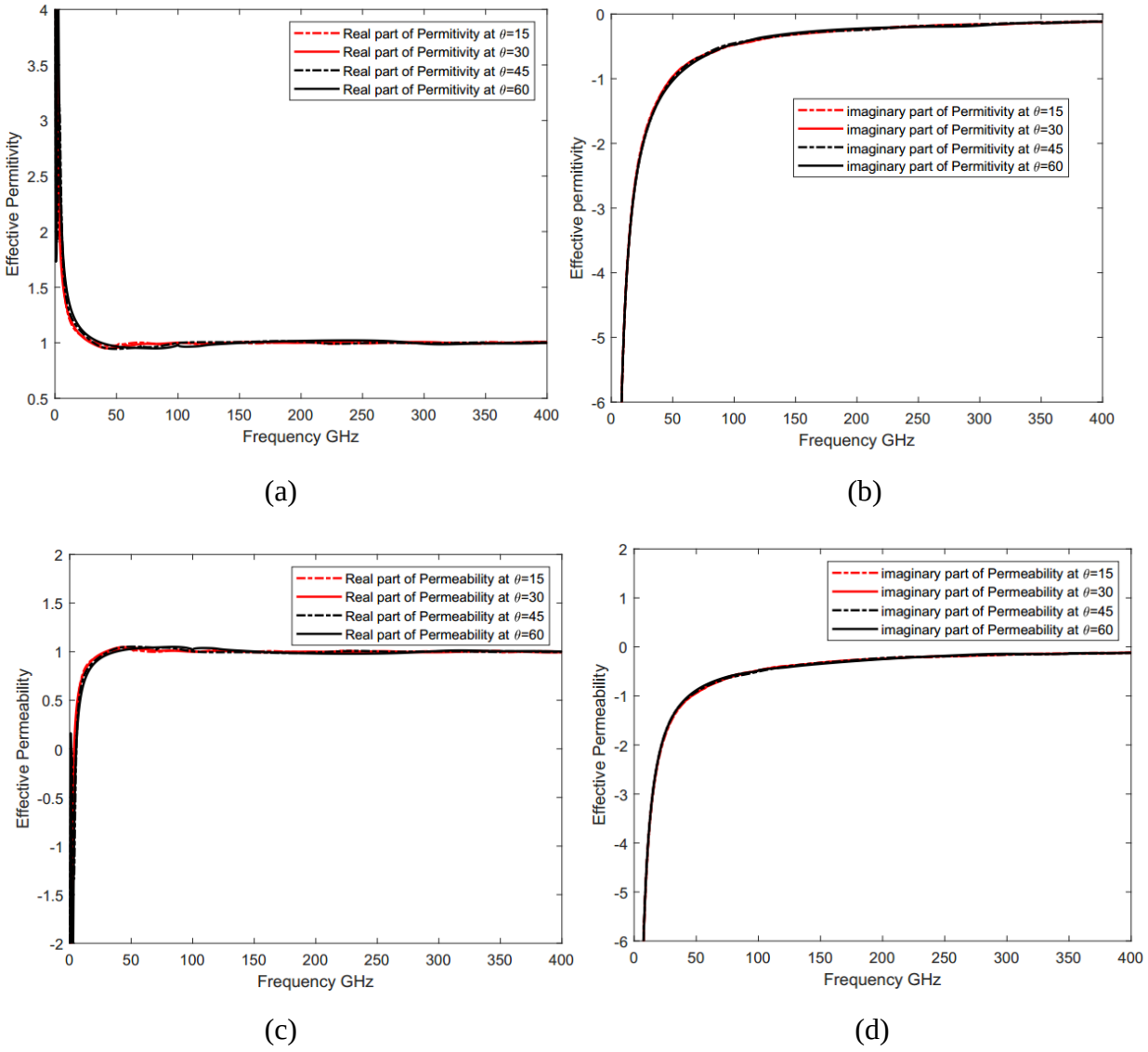

Figure 7 Extracted electromagnetic constitutive parameters at TE (a)real part of permittivity (b) imaginary part of permittivity (c) real part of permeability (d) imaginary part of permeability

Here, we examined the absorbency efficiencies of the suggested absorber under TE and TM polarizations in Fig. 5(b) and (d), respectively, for a range of polarization angles with step sizes of 30° between 30° and 180°. The absorption against polarization angle findings clearly show that the suggested absorber is insensitive for both the TE and TM modes at normal incidence. With a high absorbency of over 99 percent, the suggested meta-material can function as an absorber across polarization angles of up to 90 degrees. Moreover, it is unaffected by applied total polarization angles that increase the polarization angle. Furthermore, the suggested absorber bandwidth remains consistent across different polarization orientations.

International Journal of Computing and Engineering
ISSN 2958-7425 (online)
Vol. 5, Issue No. 4, pp. 27 - 43, 2024
www.carijournals.org

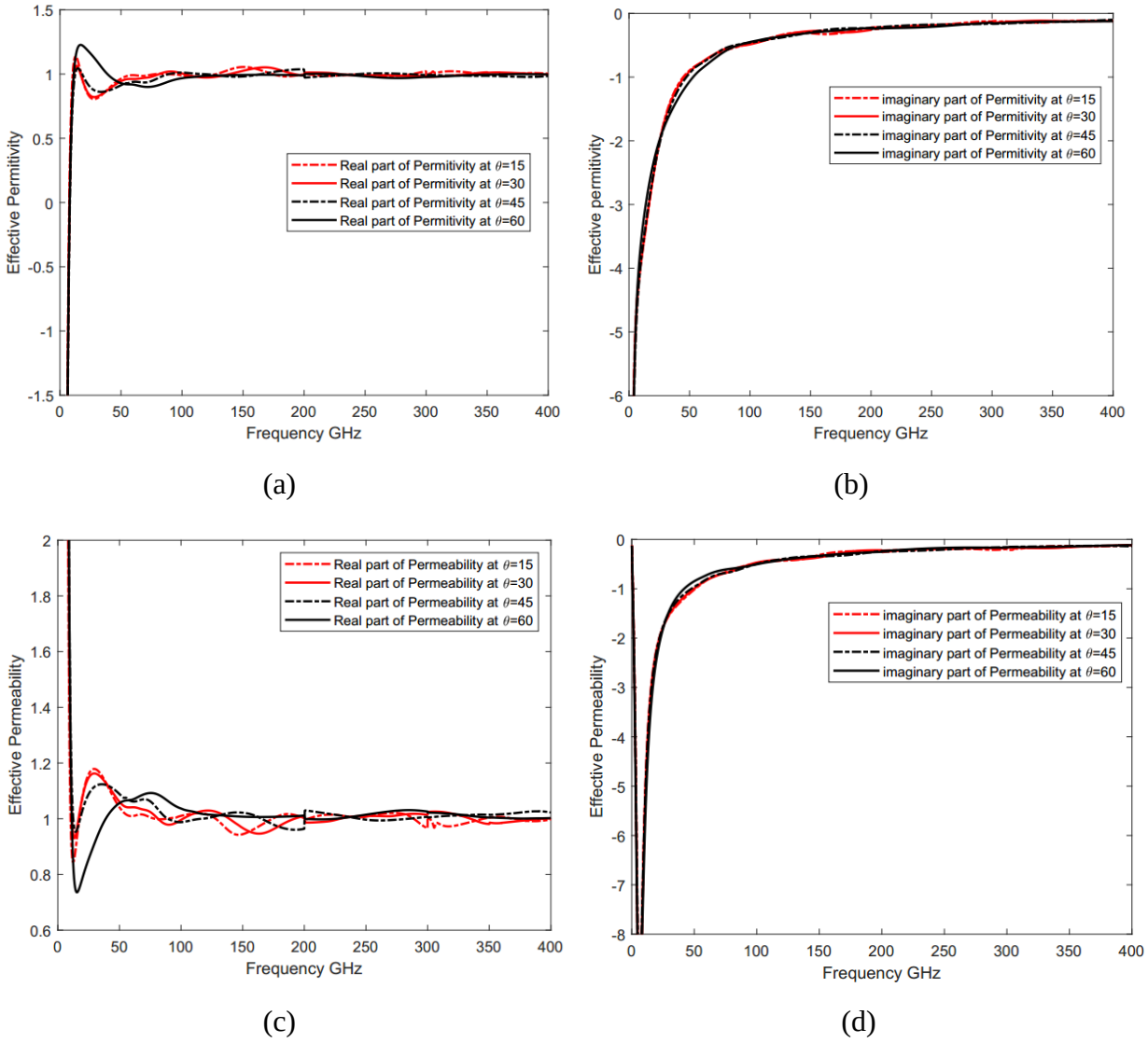

Figure 8 Extracted electromagnetic constitutive parameters at TM (a)real part of permittivity (b) imaginary part of permittivity (c) real part of permeability (d) imaginary part of permeability

We evaluated the efficiency performances of our suggested absorber with those of the other absorbers in the literature in order to assess its performance. In terms of operating band, absorption efficiency, relative bandwidth, bandwidth ratio, and thickness, the comparison is shown in Table.2. The comparative table makes it very evident that the suggested absorber offers a number of better qualities. It features angular stability across the whole operating band, a very strong absorption performance, and an extremely wide frequency range of operation. It is crucial to have an ultra-thin thickness in addition to these excellent qualities show in table.1:

International Journal of Computing and Engineering
ISSN 2958-7425 (online)
Vol. 5, Issue No. 4, pp. 27 - 43, 2024
www.carijournals.org

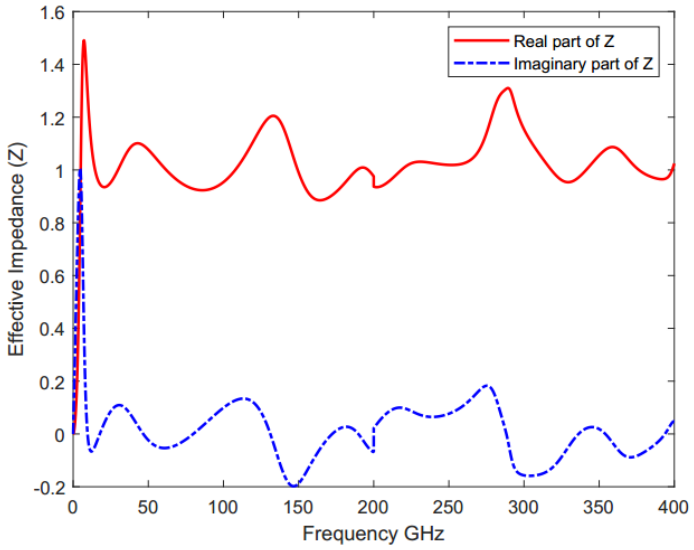

Figure 9 Extracted effective input impedance

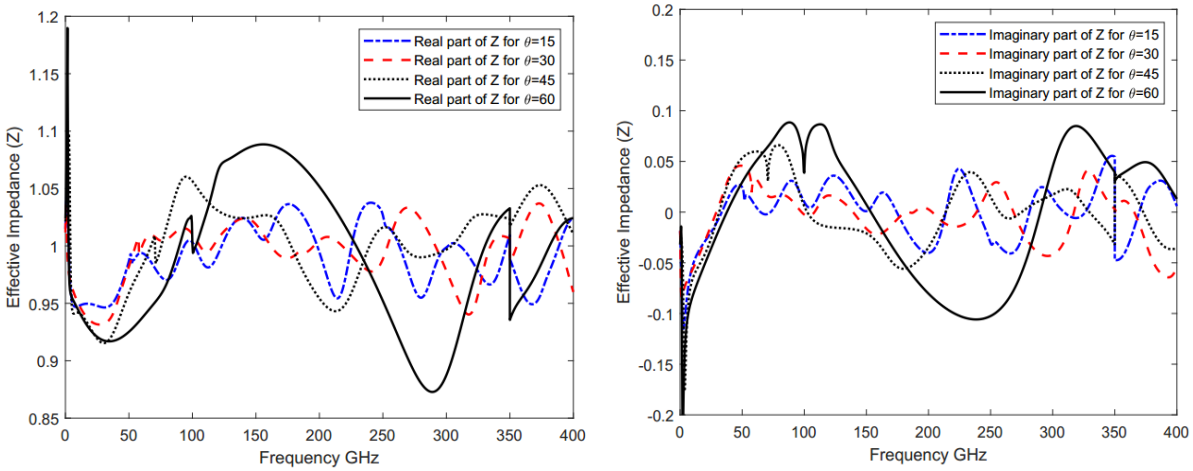

(a) (b)

Figure 10 Extracted effective input impedance at TE (a)real part (b)imaginary part

The absorption efficiencies of the design when the thickness is varied to a variety of values are displayed in Fig. 12. It is demonstrated that the thickness of 2 mm, which was selected for this design, has the maximum absorption value. Additionally, it appears that the results for thicknesses of 6 and 8 mm are identical, while the results for thicknesses of 4 mm are extremely similar.

International Journal of Computing and Engineering
ISSN 2958-7425 (online)
Vol. 5, Issue No. 4, pp. 27 - 43, 2024
www.carijournals.org

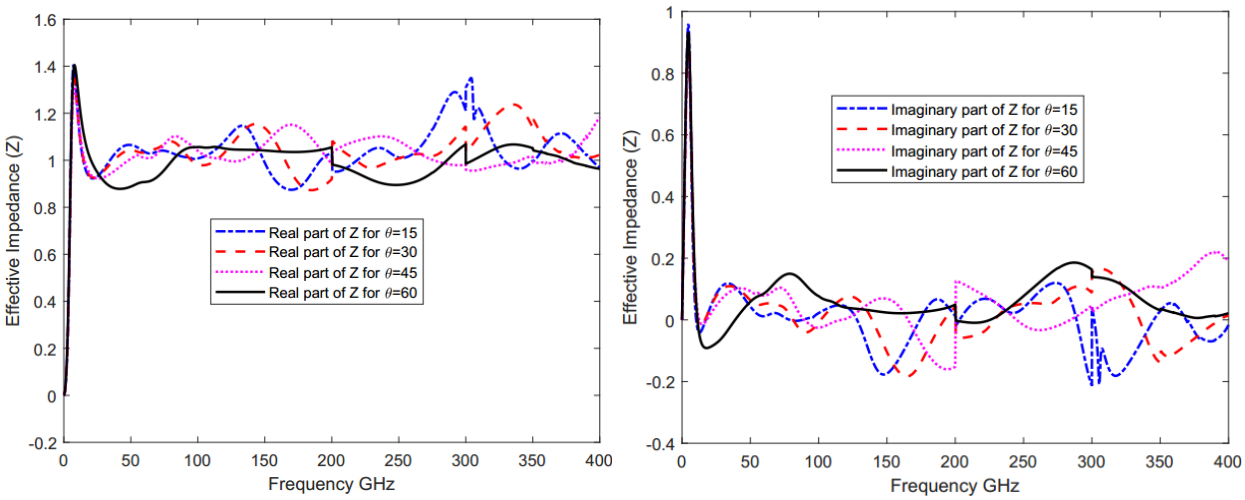

(a) (b)

Figure 11 Extracted effective input impedance at TE (a)real part (b)imaginary part

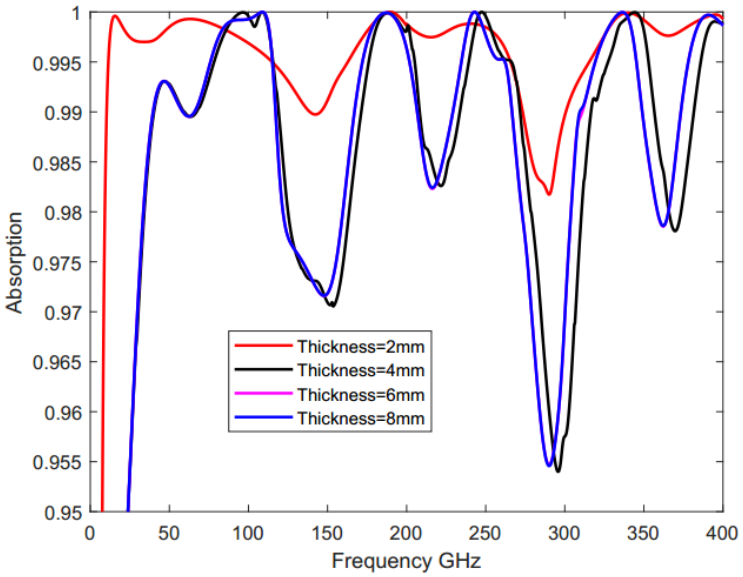

Figure 12 proposed design While the thickness value changes

Table 2 Comparison with Some Radar Absorber

Ref	Operating band (GHz)	Absorption Efficiency (%)	RBW (%)	Thickness (mm)
(Yao et al., 2020)	1 — 12.9	>90%	171.2	$0.09\lambda_0$
(Su et al., 2022)	1.5 — 40	>90%	185.5	$0.1\lambda_0$
(Zhou & Shen, 2020)	1.85 — 19.2	>90%	164.9	$0.11\lambda_0$
(J. Chen, Shang, & Liao, 2018)	2 — 17.07	>90%	158	$0.1\lambda_0$
(Tayde, Saikia, Srivastava, & Ramakrishna, 2018)	2 — 18.5	>90%	161	$0.08\lambda_0$
(X. Sun et al., 2022)	2.4 — 40	>90%	177.4	$0.15\lambda_0$
(F.-f. Li, Lou, Chen, Poo, & Wu, 2018)	3.15 — 18	>90%	140.4	$0.06\lambda_0$
(P. Chen et al., 2021)	4.73 — 39.04	>90%	156.7	$0.14\lambda_0$
(Zhu et al., 2022)	7.3 — 44.2	>90%	143.3	$0.1\lambda_0$
(F.-f. Li et al., 2018)	9 — 40	>90%	126.5	$0.08\lambda_0$
(J. Sun, Liu, Dong, & Zhou, 2011)	10 — 70	>90%	150	$0.15\lambda_0$
(Tang, Xiao, Xu, Ma, & Wang, 2016)	20 — 55	>90%	93.3	$0.6\lambda_0$
(Ling, Xiao, Zheng, Tang, & Xu, 2016)	38 — 142	>90%	115.5	$0.13\lambda_0$
(Tang, Xiao, Xu, & Liu, 2016)	58.6 — 91.4	>90%	43.7	$0.06\lambda_0$
(Coskun, Ozmen, Ahmed, & Ertugrul, 2024)	4 — 300	>99%	194.7	$0.03\lambda_0$
This work	4 — 400	>99.8	196.04	$0.028\lambda_0$

Conclusion

Angle radar absorber that can be used in millimeter band, S, C, X, Ku, K, Ka-, V, and W applications. Since no other design has outstanding absorption in all of these bands, this work adds to the body of literature. The absorption efficiency is more than 98% for the 4 GHz to 400 GHz frequency band with RBW of 196.04% when the incidence is normal. Meanwhile, even when the incidence angle is extended from 0° to 45°, the suggested design may continue to provide outstanding absorption performance. Also compare the proposed design versus thickness. Superb impedance matching and significant dielectric loss also contribute to the exceptional radar absorption efficiency. In the ultra-wide spectrum electromagnetic shielding field for radar applications, the suggested design shows promise. Researchers recommend studying the same design for curved surfaces at the same frequencies and using it to study the radar cross section reduction.

References

Cai, W., Chettiar, U. K., Kildishev, A. V., & Shalaev, V. M. (2007). Optical cloaking with metamaterials. Nature photonics, 1(4), 224-227.

Chen, J., Shang, Y., & Liao, C. (2018). Double-layer circuit analog absorbers based on resistor-loaded square-loop arrays. IEEE antennas and wireless propagation letters, 17(4), 591-595.

Chen, P., Kong, X., Han, J., Wang, W., Han, K., Ma, H., . . . Shen, X. (2021). Wide-angle ultra-broadband metamaterial absorber with polarization-insensitive characteristics. Chinese physics letters, 38(2), 027801.

Coskun, A., Ozmen, A., Ahmed, F., & Ertugrul, M. (2024). Achieving High Efficiency, Super Broadband, Ultra-Thin, and Advanced Electromagnetic Absorption for S, C, X, Ku, K, Ka, V, W, and Millimeter Band Radar Applications.

Farhat, M., Guenneau, S., Movchan, A., & Enoch, S. (2008). Achieving invisibility over a finite range of frequencies. Optics express, 16(8), 5656-5661.

Gabrielli, L. H., Cardenas, J., Poitras, C. B., & Lipson, M. (2009). Silicon nanostructure cloak operating at optical frequencies. Nature photonics, 3(8), 461-463.

Huang, C., Ji, C., Zhao, B., Peng, J., Yuan, L., & Luo, X. (2021). Multifunctional and tunable radar absorber based on graphene-integrated active metasurface. Advanced Materials Technologies, 6(4), 2001050.

Kim, J., Han, K., & Hahn, J. W. (2017). Selective dual-band metamaterial perfect absorber for infrared stealth technology. Scientific Reports, 7(1), 1-9.

Landy, N. I., & Padilla, W. J. (2009). Guiding light with conformal transformations. Optics express, 17(17), 14872-14879.

Li, F.-f., Lou, Q., Chen, P., Poo, Y., & Wu, R.-X. (2018). Broadband backscattering reduction realized by array of lossy scatterers. Optics express, 26(26), 34711-34718.

Li, J., & Pendry, J. B. (2008). Hiding under the carpet: a new strategy for cloaking. Physical review letters, 101(20), 203901.

Li, M., Muneer, B., Yi, Z., & Zhu, Q. (2018). A broadband compatible multispectral metamaterial absorber for visible, near-infrared, and microwave bands. Advanced Optical Materials, 6(9), 1701238.

Li, S.-J., Wu, P.-X., Xu, H.-X., Zhou, Y.-L., Cao, X.-Y., Han, J.-F., . . . Zhang, Z. (2018). Ultra-wideband and polarization-insensitive perfect absorber using multilayer metamaterials, lumped resistors, and strong coupling effects. Nanoscale research letters, 13, 1-13.

Lin, M., Yi, J., Chen, X., Jiang, Z. H., Zhu, L., Qi, P., & Burokur, S. N. (2021). Compact multi-functional frequency-selective absorber based on customizable impedance films. Optics express, 29(10), 14974-14984.

Ling, X., Xiao, Z., Zheng, X., Tang, J., & Xu, K. (2016). Ultra-broadband metamaterial absorber based on the structure of resistive films. Journal of electromagnetic waves and applications, 30(17), 2325-2333.

Pendry, J. B., Holden, A., Stewart, W., & Youngs, I. (1996). Extremely low frequency plasmons in metallic mesostructures. Physical review letters, 76(25), 4773.

Pendry, J. B., Schurig, D., & Smith, D. R. (2006). Controlling electromagnetic fields. Science, 312(5781), 1780-1782.

Schurig, D., Mock, J. J., Justice, B., Cummer, S. A., Pendry, J. B., Starr, A. F., & Smith, D. R. (2006). Metamaterial electromagnetic cloak at microwave frequencies. Science, 314(5801), 977-980.

Shelby, R. A., Smith, D., Nemat-Nasser, S., & Schultz, S. (2001). Microwave transmission through a two-dimensional, isotropic, left-handed metamaterial. Applied Physics Letters, 78(4), 489-491.

Shi, M., Xu, C., Yang, Z., Liang, J., Wang, L., Tan, S., & Xu, G. (2018). Achieving good infrared-radar compatible stealth property on metamaterial-based absorber by controlling the floating rate of Al type infrared coating. Journal of Alloys and Compounds, 764, 314-322.

Sista, K. S., Dwarapudi, S., Kumar, D., Sinha, G. R., & Moon, A. P. (2021). Carbonyl iron powders as absorption material for microwave interference shielding: A review. Journal of Alloys and Compounds, 853, 157251.

Soheilifar, M. R., & Zarrabi, F. B. (2019). Reconfigurable metamaterial absorber as an optical switch based on organic-graphene control. Optical and Quantum Electronics, 51(5), 155.

Su, J., Li, W., Qu, M., Yu, H., Li, Z., Qi, K., & Yin, H. (2022). Ultrawideband RCS reduction metasurface based on hybrid mechanism of absorption and phase cancellation. IEEE Transactions on Antennas and Propagation, 70(10), 9415-9424.

Sun, J., Liu, L., Dong, G., & Zhou, J. (2011). An extremely broad band metamaterial absorber based on destructive interference. Optics express, 19(22), 21155-21162.

Sun, X., Li, Y., Huang, Y., Cheng, Y., Wang, S., & Yin, W. (2022). Achieving super broadband electromagnetic absorption by optimizing impedance match of rGO sponge metamaterials. Advanced Functional Materials, 32(5), 2107508.

Tang, J., Xiao, Z., Xu, K., & Liu, D. (2016). A polarization insensitive and broadband metamaterial absorber based on three-dimensional structure. Optics Communications, 372, 64-70.

Tang, J., Xiao, Z., Xu, K., Ma, X., & Wang, Z. (2016). Polarization-controlled metamaterial absorber with extremely bandwidth and wide incidence angle. Plasmonics, 11, 1393-1399.

Tayde, Y., Saikia, M., Srivastava, K. V., & Ramakrishna, S. A. (2018). Polarization-insensitive broadband multilayered absorber using screen printed patterns of resistive ink. IEEE antennas and wireless propagation letters, 17(12), 2489-2493.

Valentine, J., Li, J., Zentgraf, T., Bartal, G., & Zhang, X. (2009). An optical cloak made of dielectrics. Nature materials, 8(7), 568-571.

Veselago, V. G. (1968). The electrodynamics of substances with simultaneously negative values of img align= absmiddle Alt= ϵ Eps/Img and μ. Physics-Uspekhi, 10(4), 509-514.

Wang, T., Ding, M.-D., He, H.-H., Mao, J.-B., & Ruan, J.-F. (2022). Ultra-wideband polarization-and angle-insensitive metamaterial absorber based on multilayer resistive ink. Journal of electromagnetic waves and applications, 36(2), 272-284.

Yang, J. G., Kim, N. J., Yeom, I. S., Keum, H. S., Yoo, Y. J., Kim, Y. J., & Lee, Y. (2017). Method of measuring the amounts of electromagnetic radiation absorbed and controlled by metamaterials in anechoic chamber. Measurement, 95, 328-338.

Yao, Z., Xiao, S., Li, Y., & Wang, B.-Z. (2020). On the design of wideband absorber based on multilayer and multiresonant FSS array. IEEE antennas and wireless propagation letters, 20(3), 284-288.

Zhou, L., & Shen, Z. (2020). Absorptive coding metasurface with ultrawideband backscattering reduction. IEEE antennas and wireless propagation letters, 19(7), 1201-1205.

Zhu, R., Wang, J., Jiang, J., Xu, C., Liu, C., Jia, Y., . . . Chu, Z. (2022). Machine-learning-empowered multispectral metafilm with reduced radar cross section, low infrared emissivity, and visible transparency. Photonics Research, 10(5), 1146-1156.

©2023 by the Authors. This Article is an open access article distributed under the terms and conditions of the Creative Commons Attribution (CC BY) license (http://creativecommons.org/licenses/by/4.0/)